The effects of pretreatment and coating on the formability of extrusion-coated multilayer paperboard–plastic composites

Franke Wilken, Leminen Ville, Groche Peter, Varis Juha

DOI: 10.1002/pts.2542

Packaging Technology and Science
An International Journal

The effects of pre-treatment and coating on the formability of extrusion-coated multi-layer paperboard-plastic composites

Journal:	*Packaging Technology and Science*
Manuscript ID	PTS-20-0030.R2
Wiley - Manuscript type:	Research Article
Date Submitted by the Author:	05-Oct-2020
Complete List of Authors:	Franke, Wilken; TU Darmstadt, Institute for production engineering and forming machines Leminen, Ville; Lappeenranta University of Technology, Mechanical engineering Groche, Peter; TU Darmstadt, Institute for production engineering and forming machines Varis, Juha; Lappeenranta University of Technology, Lut Metal Technology
Keywords:	Forming technology, Paper composite, Material analysis

The effects of pre-treatment and coating on the formability of extrusion-coated multi-layer paperboard-plastic composites

Franke, Wilken[1]; Leminen, Ville[2]*; Groche, Peter[1]; Varis, Juha[2]

[1]Technische Universität (TU) Darmstadt, PtU, Otto-Berndt-Str. 2, 64287 DARMSTADT, GERMANY
[2]Lappeenranta University of Technology, P.O. Box 20, 53851 LAPPEENRANTA, FINLAND
*Corresponding author

Abstract

Sustainable materials like paperboard can substitute for crude oil–based polymers in packaging applications and, by doing that, reduce the negative environmental impacts caused by plastic waste. For a broader application in the packaging industry, the forming of paperboard needs to overcome its limited forming behaviour and barrier properties. The presented work aims to influence the forming behaviour of uncoated and PET-coated paperboard with additives like water, gelatin and soap. Furthermore, the differences in the mechanical behaviour of coated and uncoated materials are investigated. For the studies, tensile, bulge and forming tests were combined with different optical measurement methods. The investigations showed that the overall forming behaviour is affected by the mentioned additives and can be improved. Additionally, the interaction of the coating and substrate paper is investigated under different load conditions.

1. Introduction

The three-dimensional (3D) forming of wood fibre–based materials, such as paper and paperboard, has garnered wide interest in recent years. The research and development work has been concentrated on both the mechanical aspects of the forming processes [1-6] and the development of formable fibre-based materials [7-9]. In packaging applications in particular, alternatives for packages made completely of crude oil–based polymers are sought after as the yearly amount of plastic waste generated is 275 Mt, and up to 12.7 Mt of this is estimated to end up in our oceans [10]. In order to reduce the amount of plastic waste, paper and paperboard could be a sustainable alternative. Products made of this material can be easily recycled in existing recycling systems and, if they unintentionally end up in the environment, they are biodegradable. Forming processes like thermoforming or deep drawing find rife application in plastic packaging and the metal industry. These processes are used because of their high process speed and economical material utilisation. Due to the limited extensibility of paper-based materials, comparable geometrical freedom is not given to paper-based packaging products and prevents the material from being broadly used in these processes.

Previous work regarding the forming processes has mostly been focused on process and parameter optimisation [3-4, 11-12] and tooling [1-2]. However, influencing or enhancing the formability of fibre-based materials during or before forming operations has not yet been widely studied. Influencing the moisture content of the formed material has been proven by Hauptmann and Majschak [13], as well as by Östlund et al. [14], to be of significant importance when fibre-based materials are formed three-dimensionally. Early

works by Scherer [15] suggested that using soap water or other similar lubricants could improve the forming result. The application of steam during the deep drawing of paperboard has also shown promising results with respect to the forming limits [16]. Several works have shown that using gelatin as an additive in fibre-material manufacturing can improve the extensibility and thermal formability of fibre-based materials when added in the wet stage during the paper or paperboard manufacturing process [17-19].

In packaging applications, fibre-based materials are usually coated with a polymer layer to achieve adequate barrier properties, for example, against water, grease or oxygen. The influence of the polymer coating on top of the fibre-material is known to have a great influence on the barrier properties of the material, such as the oxygen transmission rate (OTR) or oil and grease permeability [4, 22-25]. Furthermore, improvements to the forming and die cutting processes [22-25] and changes to the coating material that increase the biodegradability of coated paperboard have been gained [23-25].

However, its influence on the mechanical properties in 3D-forming for packaging applications has not been widely investigated, although the presence of the coating presumably also has an effect on the mechanical formability of the materials.

The aim of this paper is twofold:

i. It aims to investigate the interaction of the coating layer and the substrate paperboard in multi-layer paperboard-plastic composites regarding the formability. The studies were made on coated and uncoated material, and also on a separated extrusion coating layer in order to compare the results of the different material tests.
ii. The investigations are further used to affect and optimise the composites' formability and extensibility by the use of different additives.

2. Materials and methods

Materials

The substrates used in the experiments are Stora Enso (Finland) Trayforma Performance 350, a paperboard with a base material grammage of 350 g/m^2 (TFn), and Trayforma Performance 350 + 40 WPET (TFc), which has an extrusion coating of 40 g/m^2 polyethylene terephthalate (PET) but is otherwise identical to TFn (Figure 1). The basic paperboard consists of two solid-bleached sulfate (SBS) layers, with a chemo-thermo-mechanical (CTMP) layer between them. The main component of the substrate is hardwood fibre with an alkyl ketene dimer (AKD) hydrophobic sizing additive. The fibre dimensions of the paperboard are measured using an L&W Fiber Tester (ABB, Stockholm, Sweden). The fibre length, fibre width and kink index are measured at 1.1 mm, 22.5 µm and 1.13 mm^{-1} respectively. Herein, the kink index indicates the number of kinks (changes in fibre curvature greater than 30°) divided by the total fibre length of all investigated fibres. The material represents a commonly used paperboard grade in industrial paperboard tray and plate production.

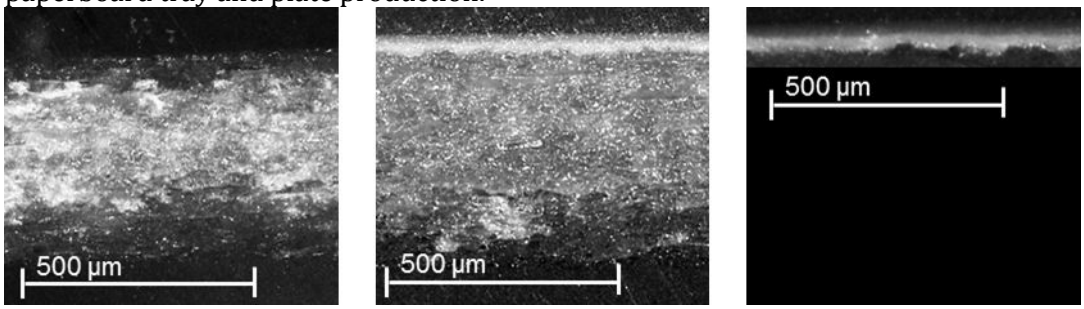

Figure 1: Images of the material section: TFn (left), TFc (middle) and the PET coating (right)

To influence the material's behaviour during the process, Scherer [15] and Vishtal et al. [19] described the influence of soap and gelatin on the extensibility of paperboard. Scherer [15] used soap in a cup drawing test to reduce the inner and outer friction. Within the investigations of Vishtal et al. [19], gelatin was mixed into the pulp for making paperboard with a higher extensibility. On the basis of these investigations, soap and gelatin were used to influence formability in the present work. For this purpose, standard gall soap and pig-based gelatin were used. Due to the water solubility of these influencers, water will be used as substrate and reference.

Methods

In the following chapter, the methods used to prepare the materials and specimens, the material conditioning, the test methods and the analysis methods will be described. The determination of the influence of the coating and the additives on the mechanical behaviour of the material tensile tests was performed in a machine direction (MD) and in a cross direction (CD) for each material and additive composition. Additionally, bulge tests were carried out to understand the influence of different stress states. Finally, the influence on industry-related processes was evaluated by forming prepared specimens in a stretch-forming test.

The separation of coating and fibres

Due to the manufacturing process of the coated paperboard by extrusion coating, the coating itself is not available as a single-layer material foil. Thus, the paper fibres have to be separated from the coating in order to test the coating itself. This separation is done by soaking the coated material in water for 24 hours. After this time, some fibre layers can be manually removed from the coating. Further fibres are then carefully brushed off with a soft hand brush. At the end of this process, only single fibres are still sticking to the coating, visible in Figure 2. Furthermore, it is obvious that the fibres have no direct contact with each other, which excludes the effect of inter-fibre bonding forces.

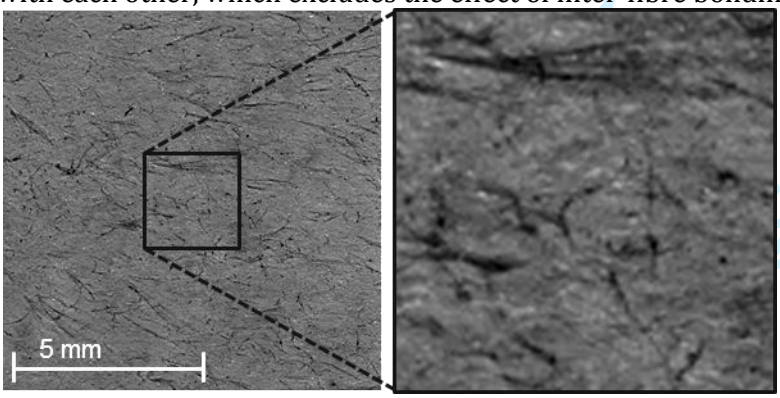

Figure 2: The surface of the separated coating layer (view from the former paperboard side)

The application of additives

For the pre-conditioning of the specimens, water-based solutions were prepared. According to the findings in [15], the soap solution preferably has a mass content of soap of 1.6 %. In [19], the pulp for making the paper blanks was infused with 4 % of gelatin. This showed a positive effect on the extensibility of the material. Preliminary tests showed that the conditioned samples with gelatin solution stuck together. This effect is already detectable with a 0.4 % solution of gelatin, which is the reason for using this mass content. The three influencing solutions (water, the soap solution, the gelatin solution) were applied to the specimens to adjust a moisture content of 20 % (mass) by the use of a spray can. To homogenise the conditions applied, the specimens were stored for at least 24 h in a controlled manner. The specimens were immediately tested after removal from the

storage. Furthermore, to suppress the influences of room conditions, all specimens were tested under the same conditions.

The tensile test

The tensile test specimens were cut out of a blank by a shear cutting machine according to DIN EN ISO 1924-2, which implies that the specimen length is 180 mm (±1 mm), the width is 15 mm (±0.1 mm) and the pulling speed is 20 mm/min (±5 mm/min). Due to the restrictions of the tensile test machine (ZwickRoell AllroundLine Z100), the measuring length of the specimen was chosen to be 116 mm (±7 mm). By using an external video extensometer, influences due to machine compliance could be avoided. The specimens were mechanically clamped in the tensile test machine.

The bulge test

Huttel et al. [20] described a self-built bulge test setup which is transferred from a hydraulic bulge test according to ISO 16808 for the characterisation of metals to paper-based materials. The test procedure starts with the clamping of the specimen in the circular direction (Figure 3 – Preparation). After the clamping, pneumatic pressure is applied above the plastic foil, which transfers a homogeneous pressure onto the bottom side of the test specimen. During the test procedure the pressure is linearly increased until the specimen bursts. A camera observes the surface for subsequent strain calculations (Figure 3 – Test).

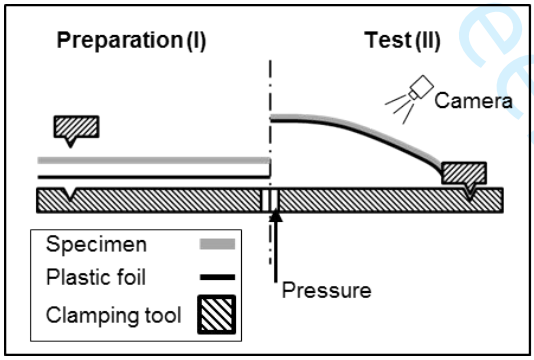

Figure 3: The schematic bulge test setup

For this material characterisation procedure, circular blanks with a diameter of 200 mm were cut out of the sheets and prepared according to the test parameters. Additionally, a graphite-based speckle pattern was applied to the upper side of the specimen. This pattern was used by the optical strain measurement system, GOM's Aramis, to determine the strain distribution on the surface. For the evaluation of the strain on the surface, the strain in the MD and CD were averaged along a linear path on the specimen (Figure 4) [6]. The left side of Figure 4 shows the surface of a bulged specimen immediately before the bulge bursts. Herein the greyscale represents the displacement in the *z*-direction in order to find the highest area. According to Huttel et al. [20] and ISO 16808, it is assumed that the highest strain occurs in the middle (the highest area) of the specimen. The measured section strain is calculated via GOM's Aramis Software and is shown on the right side of the figure. This diagram exemplarily displays the strain in the *y*-direction (epsilon *Y*) of the camera system. By aligning each specimen according to that coordinate system, influences on the measurement values by the test apparatus or the measurement system could be eliminated.

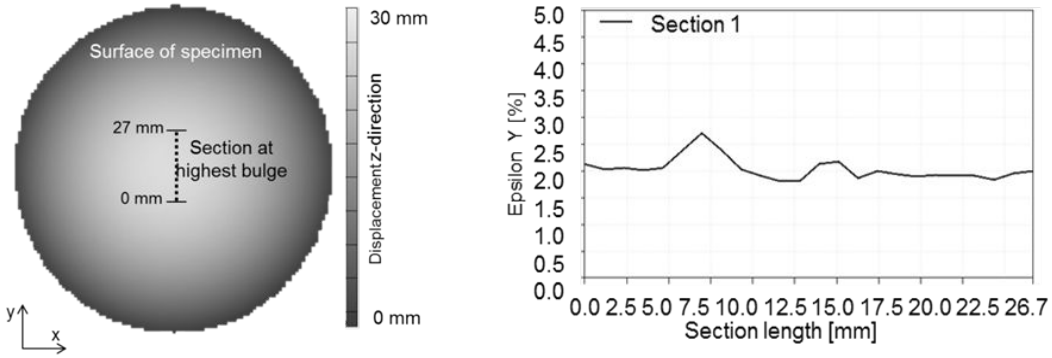

Figure 4: The definition of the section and calculation of the mean value of strain – section adjustment by displacement in a *z*-direction (left) and calculation of the mean value (strain) along the section (right)

The multi-axial loading during the bulge test resembles the mechanical loading in many forming processes. In particular, forming processes like press forming or deep drawing exhibit regions with similar load conditions. This is why the bulge test is suitable as a multi-axial material test and allows for the prediction of the forming behaviour in industrial processes. Compared with the biaxial testing used by de Ruvo et al. [26] and Wahlström and Fellers [27], as well as Linvill and Östlund [28], this testing process is closer to industrial forming processes. The load conditions during the testing process are similar to stretch forming processes, and through that, they allow the better prediction of formability.

Forming tests – press forming

Similar to the approaches in [21], forming tests on an industrial forming machine were performed to transfer the material characterisation from laboratory scale to industrial processes and show the effect of different treatments in industrial applications. For these tests, a press forming tool set with rectangular geometry was used (Figure 5). Due to the aim of this test – determining the formability of the material – the blanks were fixed by the blank holder. The tests were performed starting with low drawing depths. Subsequently, the depth was increased until cracks occurred. The last depth without cracks is defined as a condition at the forming limit. The depth is defined by the displacement of the punch and results in a height (measured from flange to bottom; see Figure 5) in the formed part.

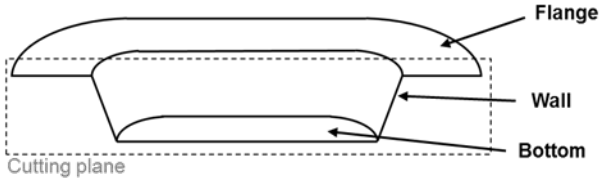

Figure 5: A schematic definition of the drawing test parts

3. Results and discussion

All the tests for each parameter setting were carried out at least five times. The error bars represent the absolute maximum and minimum values of the test series. Furthermore, force signals (tensile test) and pressure signals (bulge test) were used as comparative strength data in addition to stress. This is necessary in order to stay comparative to the superposing comparisons shown in Figure 6 and Figure 13. All experiments were carried out at the same room conditions (23 °C and 40 % relative humidity).

The tensile test

Figure 6 presents the maximal achieved forces in the tensile tests at room conditions (moisture content of the material: 5 %) with the coated and the uncoated TF material as well as the PET-coated material itself. Surprisingly, adding the maximum force values of the coating and TFn does not sum up in the values of TFc. Between the pulling force of the TFc and TFn+coating a significant difference occurs of 45 N (9.5 %) in the MD and 34 N (15.4 %) in the CD. These differences cannot be explained by inaccuracies created by the separation of the coating layer. This force difference is suggested to occur because of interactions between the PET coating layer and the paperboard itself. Due to the coating process, the PET infiltrates the fibre network of the paperboard (as implied in Figure 1) and thus strengthens the fibres and matrix compound.

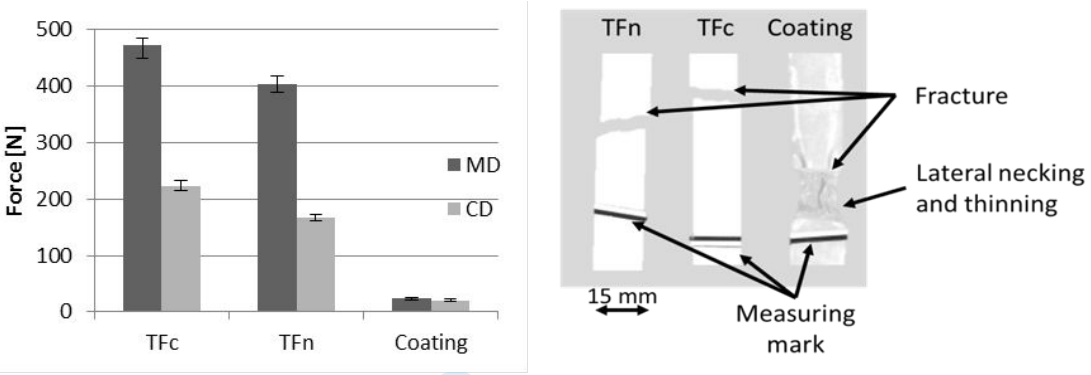

Figure 6: Average force at break of the tensile tests of TFc, TFn and the coating in an MD and CD (left) and the exemplary fracture areas of TFn, TFc and the coating (right)

Immediately after rupture, the forces decrease rapidly. This event is used to determine the points of maximum force and elongation. The maximum elongation (see Figure 7) is related to the initial measuring length of 116 mm (±7 mm) for each specimen and represents the strain immediately before rupture occurs. Obviously, the anisotropy of the material influences the strain at break and force values. In the MD there is no difference in the strain at break of TFc and TFn. On the contrary, in the CD TFn bears slightly more but, concerning the error bars, the difference in strain is negligible. The PET coating shows no anisotropy in strain compared to the TFn and the TFc material. Taking into account the thickness of the material (see Figure 1), the mean values of the bearable stress of the PET coating differ slightly. Due to the error bars, the PET coating can be seen as isotropic. However, the PET coating itself withstands smaller strains at break than TFc and TFn. After the tensile test, all the specimens were analysed regarding their geometry. The result is exemplarily shown in Figure 6 (on the right). No difference between TFn and TFc could be detected. Furthermore, the tensile test coating specimens tended towards lateral necking (the Poisson effect) and thinning around the fracture area. Lateral necking of the TFn or TFc specimens was not detected. Considering the material thickness, the stress values underline the findings from Figure 6. The combined material is able to take more stress than the sum of its components' contributions. This leads to the conclusion that the combined layers show a mutually strengthening effect. Besides the mutual supporting inside of the inter-material zone, the substrate paper layer suppresses the lateral necking of the PET coating. This is assumed to be the reason for a higher force as well as the higher tensile strength of TFc.

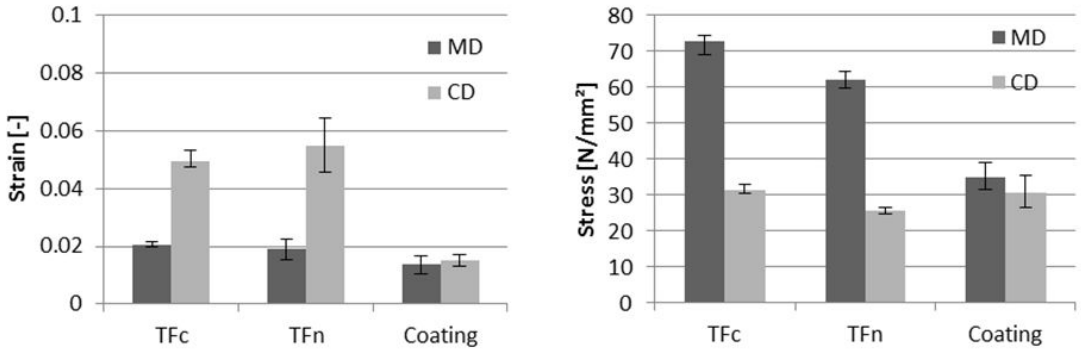

Figure 7: Average strain and stress at break of the tensile test of TFc, TFn and coating in the MD and CD for room conditions

Regarding Young's modulus, the MD values of TFn and TFc do not differ a lot in the MD but vary slightly in the CD. The Young's modulus of the coating shows no significant anisotropy and its values are at the level of the TFc and TFn in both the CD and MD. Calculating the combined Young's modulus of TFn and the coating after Equation 1 (the rule of mixture), the calculated value in the MD, $E_{calc,MD} = 6787 \frac{N}{mm^2}$, is between the error bars of the measured value of TFc. Herein E_i represents the elastic modulus of the material layer, i = 1,2, with its thickness t_i. In the CD, the calculated value $E_{calc,CD} = 2701\ N/mm^2$ is a slight underestimation of the measured value. This agrees with the combination of forces in Figure 6. The reason for the difference in the MD and CD could be found in the distinctly stiffer behaviour in the MD, which has a longer, almost linear, elastic part. In the CD the tensile behaviour differs a lot from classic linear elasticity.

$$E_{calc} = \frac{E_1 t_1 + E_2 t_2}{t_1 + t_2} \qquad \text{Equation 1}$$

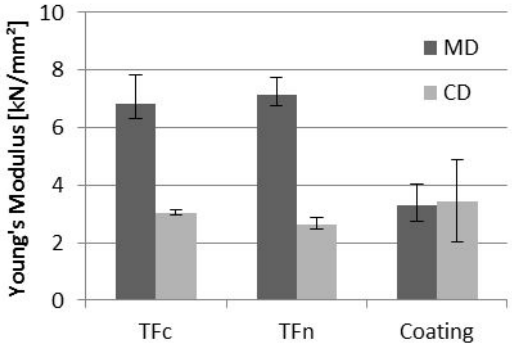

Figure 8: Young's modulus of the reference materials

The following results show the influence of adding the water, soap solution and gelatin solution on the mechanical behaviour in the tensile tests of TFn (Figure 9) and TFc (Figure 10). As can be seen in Figure 9, and as is known from literature, applying water to the uncoated material increases the strain at break but lowers the tensile strength level. Since gelatin and soap are in solution in water, this assertion also applies to them. Nevertheless, there are some differences to pure water even though there seems to be no influence of soap on the strain at break. It lowers the stress level to below 25 N/mm^2 compared with pure water-treated specimens. On the contrary, gelatin treatment increases the strain at break and decreases the tensile strength slightly, but less than soap. A lower inner friction

due to soap treatment was assumed by Scherer [15] and could explain the lower stress. The gelatin in solution infiltrates the fibre system and reinforces the crosslinking [17]. This is assumed to increase the elongation of the fibres, which leads to higher strain on the TFn.

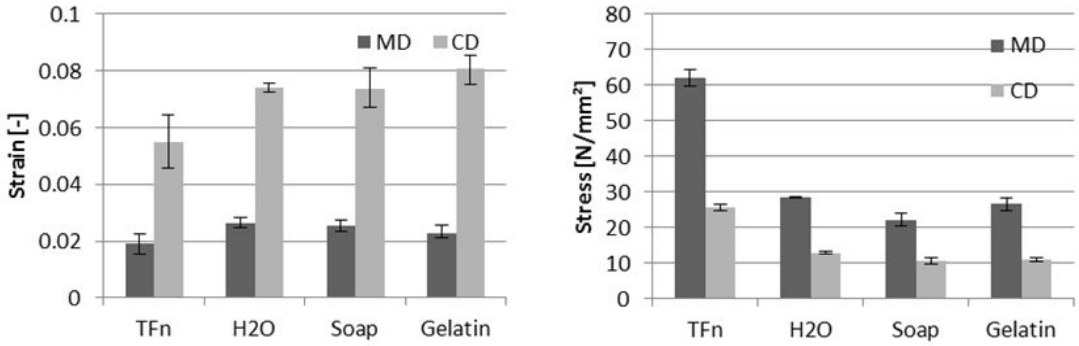

Figure 9: Average strain and stress at break of tensile tests of the uncoated reference material (TFn) and the treated materials (H2O; soap; gelatin)

The TFc material reacts to water treatment in almost the same way as TFn. But on the contrary to TFn, the additions increase neither the strain at break nor the tensile strength. Both additions decrease the strain at break as well as tensile strength values (Figure 10). This might be explained by the macroscopic, two-layered (in this case, three-layered as the paperboard counts as one layer) inhomogeneous structure in which the PET coating is not affected by soap or gelatin. Rather, the water softens the paper layer(s) but does not change the PET properties significantly. Thus, the ratio of contributions to the mechanical behaviour from both layers is changed. According to this change of ratio, the lateral strain of the coating has a higher influence on the fibre network. Furthermore, the water additives could harm the aforementioned support of the fibre network by the coating. The bonding of PET and fibres could be weakened.

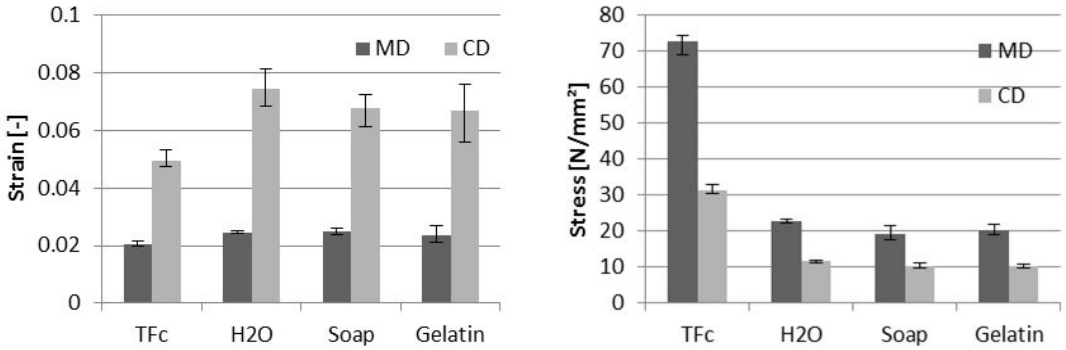

Figure 10: Average strain and stress at break of the tensile tests of coated reference (TFc) and treated materials (H2O; Soap; Gelatin)

In order to get a fast and sufficiently accurate impression of the influence of the treatment on the elastic-plastic behaviour, Young's modulus is taken into regard. The treated tensile test values differ from the reference materials. Thereby, the basic ranking stays the same, but the ratio of CD to MD differs significantly from the references to the treated tests, as depicted in Table 1. For TFn, Young's modulus decreases below half of its value in the MD by adding water, gelatin or soap. In the CD the decrease is even higher, which results in the earlier beginning of the plastic deformation. Thus, the treatment leads to very small or unmeasurable pure elastic behaviour in the CD.

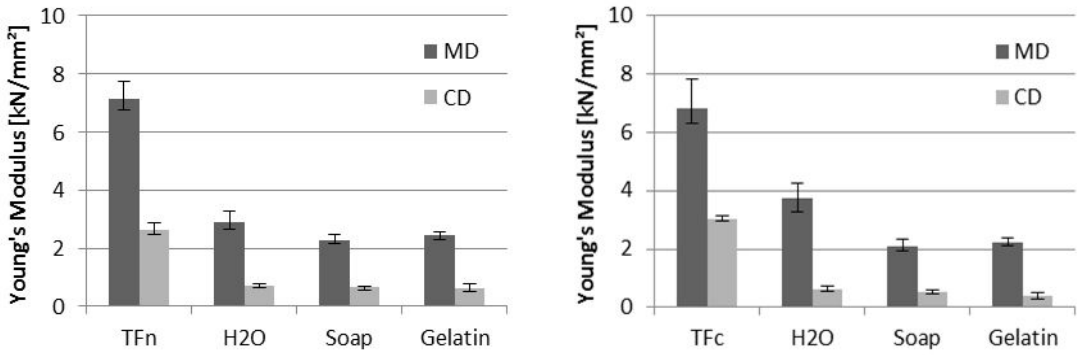

Figure 11: The Young's moduli of the references (TFn; TFc) and the treated materials (H2O; soap; gelatin)

Furthermore, the TFc ratios (see Table 1) are more affected by the treatment as TFn compared to the reference. This is in line with the tensile stress data. In particular, the Young's modulus ratios of TFc are affected by the treatment. This leads to the assumption that the treatment affects the inter-material zone more in the CD than in the MD. By adding water and solutions, hydrogen bonds are loosened. These bonds are responsible for the inter-fibre crosslinking. The strength and stiffness in both directions is dependent on these bonds. Due to more fibres being aligned in the MD as in the CD, the crosslinking of fibres is more important for strength and stress in the CD. Taking into account the inter-material zone, single fibres are embedded into the matrix material (the PET coating) and thus are hardly affected by the additives. This effect is to be found in the MD. Against that, the inter-fibre bonds (the crosslinking) can be affected by the additives and thus be loosened. The coating itself is hardly affected by the treatment, but the inter-material zone is weakened as well, which additionally reduces the mutual support (compare the Poisson effect of the PET coating above) of the two material layers.

Bulge Test Results

Figure 12 shows the average strain values (compare them with those in Chapter 2) of bulge-tested TFc, TFn and the PET coating in the MD and CD. Similar to the tensile test results, the coating withstands the lowest strain, and the values in the MD and CD do not differ significantly. Unlike the tensile test results, TFc withstands the highest strain in the MD and CD. The reason for that is assumed to be the aforementioned support of the fibre matrix by the coating. In this biaxial stress state (circular loading and clamping), the lateral elongation, which leads to earlier cracks in tensile tests, is suppressed and leads to higher strains of the TFc in bulge tests. Additionally, the coating which is by the results of the tensile tests assumed to be isotropic, contributes a more homogeneous strain distribution. This can be seen by the slightly lowered difference from MD to CD comparing TFc and TFn strain data in Figure 12. Nevertheless, the strain in the MD that occurs in bulge tests is similar, but in the CD it is less than in the tensile tests. This phenomenon can also be explained by the biaxial load situation, which leads to a homogeneous strain distribution. This distribution is caused by the circular clamping and the homogeneous pressure application, which is transmitted via the elastic foil below the specimen. In addition, the failure of the whole specimen occurs when the strain at break is reached in the least stretchable direction. This direction is the MD and explains the similar maximal elongation for the tensile and bulge test, as well as the lower elongation in the CD.

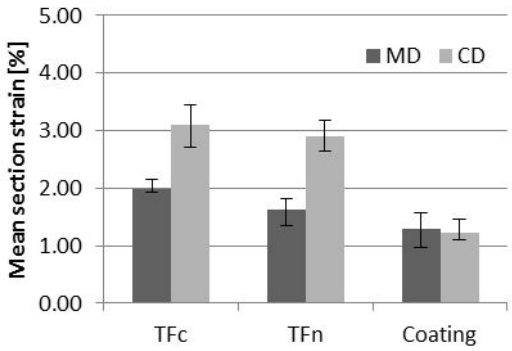

Figure 12: The values of the average strain along the section through the bulge before it bursts in a bulge test

Figure 13 shows the pressure values of the bulge test (on the left) which is congruent to Figure 6. Similar to the tensile test, the TFc withstands the highest pressure and the coating withstands the lowest pressure, which could be easily explained by the material thickness. A differentiation between the MD and CD is not necessary because of the test setup. The difference of the pressure at burst of TFc and the sum of the pressure of TFn and the coating is in contrast to the tensile test results negligibly small. This suggests that there is different interaction behaviour of the two materials in different stress conditions. In detail, uniaxial stresses (tensile test) lead to higher interaction of the materials than they do in multi-axial load conditions (bulge test). In the tensile test, the lateral necking of the coating material results in higher forces of TFc than the sum of the forces of its parts. Under a multi-axial load in the bulge test, this necking is blocked by the biaxial clamping. Furthermore, it leads to biaxial elongation which results by regarding Figure 6 (on the right) in a thinning of the coating layer. Thus the TFc material in the bulge test is weakened and the combination of its part layers does not lead to higher strength than the sum. Nevertheless, the mutual support of both materials leads to slightly higher strains for TFc (see Figure 14).

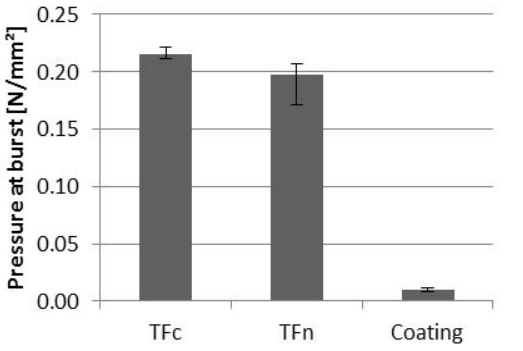

Figure 13: Pressure at burst in the bulge test for TFc, TFn and Coating

Contrary to the observations in the tensile tests, soap and gelatin solutions increased the strain in the MD for TFn in the bulge tests, which can be seen in Figure 14 (on the left). Water does not change the value of the strain in the MD but it lowers the strain in the CD to the level of the MD strain. In the CD there is additionally a decrease of strain that is measurable for soap solution–treated specimens. For the gelatin-treated specimens, the CD strain varies not measurable from the reference. As described, all the treatment solutions lower the difference between the MD and CD. Lowering the strength of paper due to higher moisture content is well described in literature [5-6, 9, 15]. Under the multi-

axial load, lower strength leads to bursting of the material at an earlier stage of straining. Adding soap or gelatin to the water means that this effect is not so strong. An explanation may be found in the bonding of soap molecules, as well as gelatin molecules, to the water, which could result from being bonded to the additives molecules, not to the loosened hydrogen bonds of inter-fibre bonds. Additionally, soap could reduce the inner friction, as assumed by Scherer [14], which would result in less resistance in the relative movement of not-bonded areas. Against that, the gelatin could strengthen the inter-fibre bonds. The results of the gelatin solution–treated bulge tests support the hypothesis and explanation of [19], namely that the added gelatin strengthens the inter-fibre bonds. Due to the multi-axial load, the inter-fibre bonds are more present compared to the tensile test results.
For TFc, the aforementioned effects are not ascertainable (see Figure 14, on the right). The strain in the CD is not significantly affected by the additions. Nevertheless, the strain in the MD can be increased by the additives and consequently reduce the anisotropic ratio. Due to the fact that the PET coating of TFc absorbs no water, the ratio of paperboard and coating to the strain changes, as it does in the tensile tests. This could additionally support the more homogeneous strain distribution in plane by a more symmetric material behaviour in the *z*-direction.

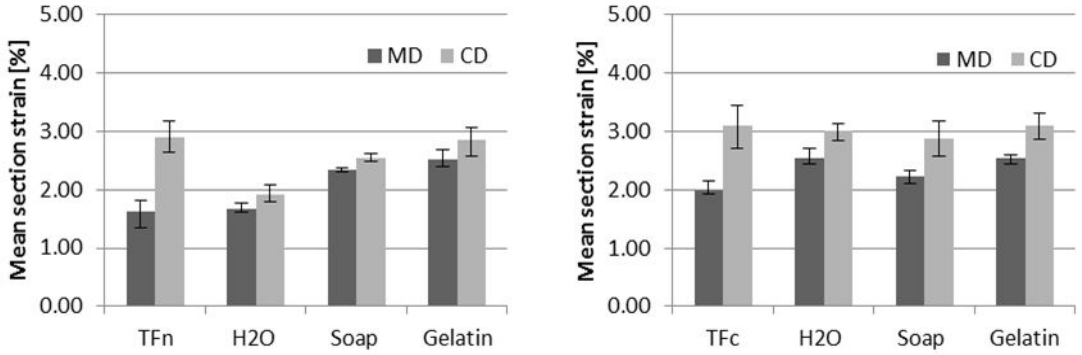

Figure 14: The bulge test results for the treated materials' strain

As mentioned before, the pressure at burst data presented in Figure 15 are used as a force equivalent value for the bulge test. Similar to Figure 13, a differentiation between the MD and CD is not necessary due to the test setup. The results are separated into TFn and TFc, where the coated material has a higher strength than the uncoated material. The untreated material has the highest pressure at breakage: 0.2 N/mm^2. All additives for the paper treatment lower the pressure by at least half (running up to a quarter), which is a higher decrease in strength compared to the tensile test. For TFn the strength increases from water, to soap, to gelatin. This is similar to the behaviour shown in Figure 14 (on the left). In the case of TFc, there is a decrease from water to soap and an increase to gelatin. Furthermore, the TFn is more affected by the additives than TFc, which could be explained by the coating layer, which is not affected by the water solutions.

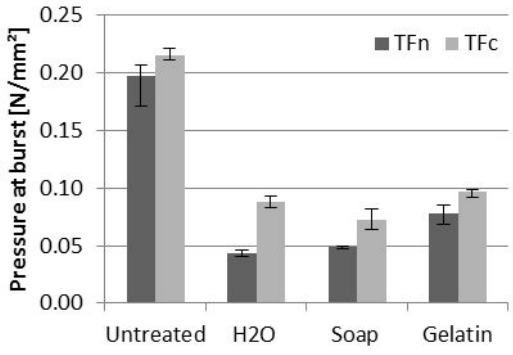

Figure 15: The bulge test results for treated materials strain

Forming test results

As mentioned in Chapter 2, a formed part with cracks on its surface is rated as a failure. These cracks develop, ranging from a low depth on the top layer of the material up to very deep cracks running through the whole material thickness (see Figure 16). Furthermore, the cracks can be located at the bottom of the formed part or on the wall (see Figure 5).

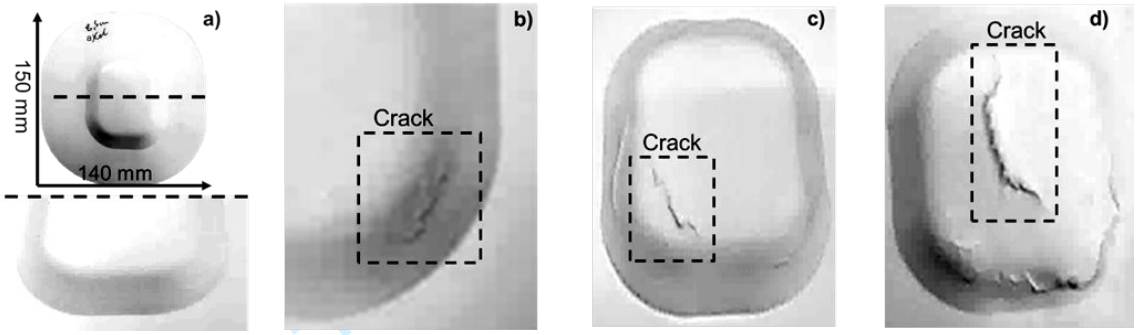

Figure 16: The fracture behaviour of the formed parts compared with parts without cracks (a), with a crack in the top layer at the flange (b), with a crack through several layers on the top (c) and with a crack through the whole thickness (d)

Apart from the cracks, which count as product failure, product imperfections develop during the forming process. Wrinkles occur in the flange area and are sometimes pulled into the wall area (see Figure 17). These phenomena are known from metal forming processes. Due to the tapering of the blank by the forming process, tangential compressive stress occurs in the flange area. This stress leads to wrinkling, which is normally suppressed by forces applied by the blank holder. In paper and paperboard forming processes, like deep drawing and press forming, the occurrence of wrinkles is accepted due to the difference in material forming behaviour (cf. [5]). A second imperfection occurring on the bottom surface on the inside is blistering. Due to the moisturising of the coated blanks, compressive stresses in the bottom lead to the delamination of paper and coating layers, which results in PET blisters.

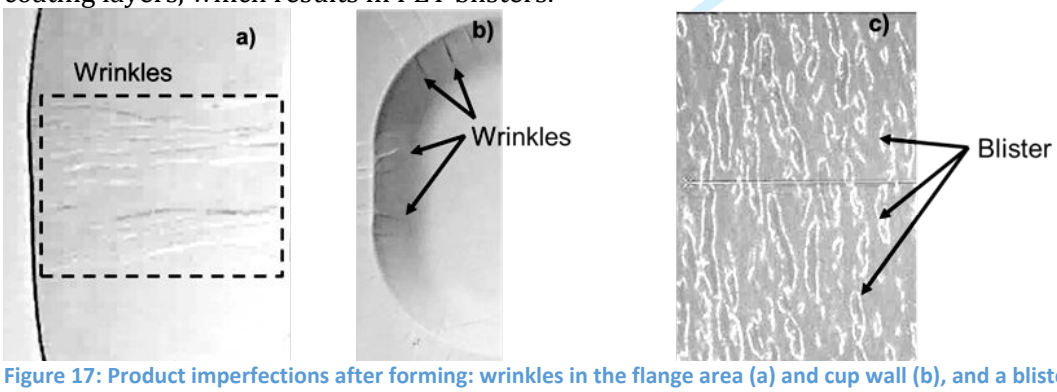

Figure 17: Product imperfections after forming: wrinkles in the flange area (a) and cup wall (b), and a blistering pattern in the bottom area (c)

Figure 18 describes the forming test results (as described in Chapter 2). According to the tensile and bulge test results, the references TFn and TFc are at the same level of drawing depth. Adding water decreases the drawing depth for both materials. This is similar to the decreasing strength in the bulge test but not to the strain behaviour. Due to the full clamping of the blank in the blank holder area, the material strength is the more important value in order to evaluate the forming behaviour. Soap in the water decreases the drawing depth further for TFn but increases the drawing depth for TFc. In the case of adding

gelatin, the deepest drawing depth could be reached for both materials. The explanation for this may be found in the bulge test data, where gelatin water–treated specimens have the combination of the highest bearable strain in the MD and CD, and the highest strength (besides the untreated material). Nevertheless, it can be pointed out that for forming prediction, even in a non-sliding toolset, the tensile strength and the strain at break are not the only parameters which should be considered. These findings underline the statement that there are many factors to consider when evaluating the formability of materials in industrial conditions. But the bulge test gives a first indication of the formability, which is additionally affected by several other factors (e.g. forming parameters, geometries, conditions and friction) [1-3, 5, 8-9, 14]. Therefore, the bulge test strain data seems to be an especially good approximating value for the forming result in an industrial toolset.

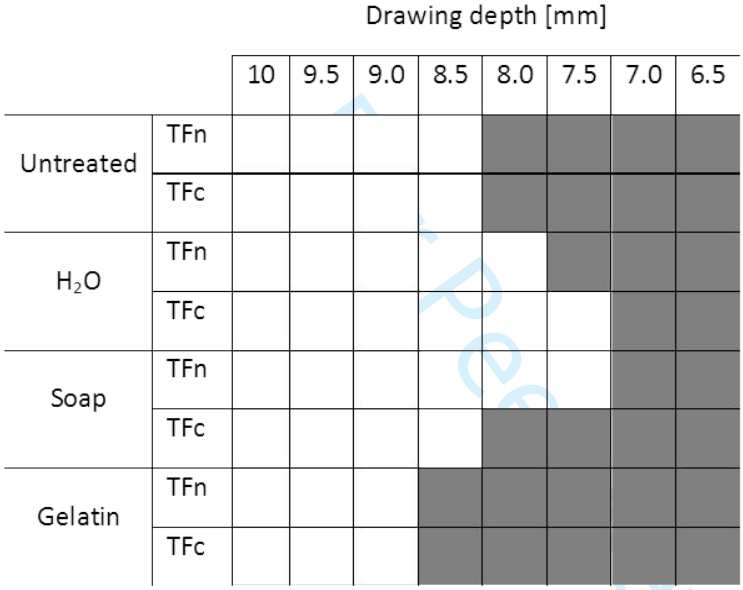

Figure 18: The forming test results for 10 mm to 6.5 mm drawing depth and all the treated and reference materials; white = failure/crack; grey = no failure/crack

Moreover, the drawing depth is not the only parameter which describes the quality of the forming results. Apart from the findings presented in Figure 18, a surface analysis was performed with a Keyence CV-5000 microscope. It showed that the formed, untreated materials have wrinkles higher in the flange area of the drawn shape than the treated materials (see Figure 19). They have lower and more homogeneously distributed wrinkles, which can be explained by the decreased bending strength of the material due to the higher moisture content. The additive in the water leads to an improved surface quality. This results in lower and fewer wrinkles for both soap and gelatin. Beyond that, the coating seems to support wrinkling with higher/deeper depth and inhomogeneity. This effect may be traced back to the different elasticity and strength of the two macroscopic material layers (paperboard and PET). Due to the lower elastic modulus of the PET coating, the board has less resistance against wrinkling on its coated side.

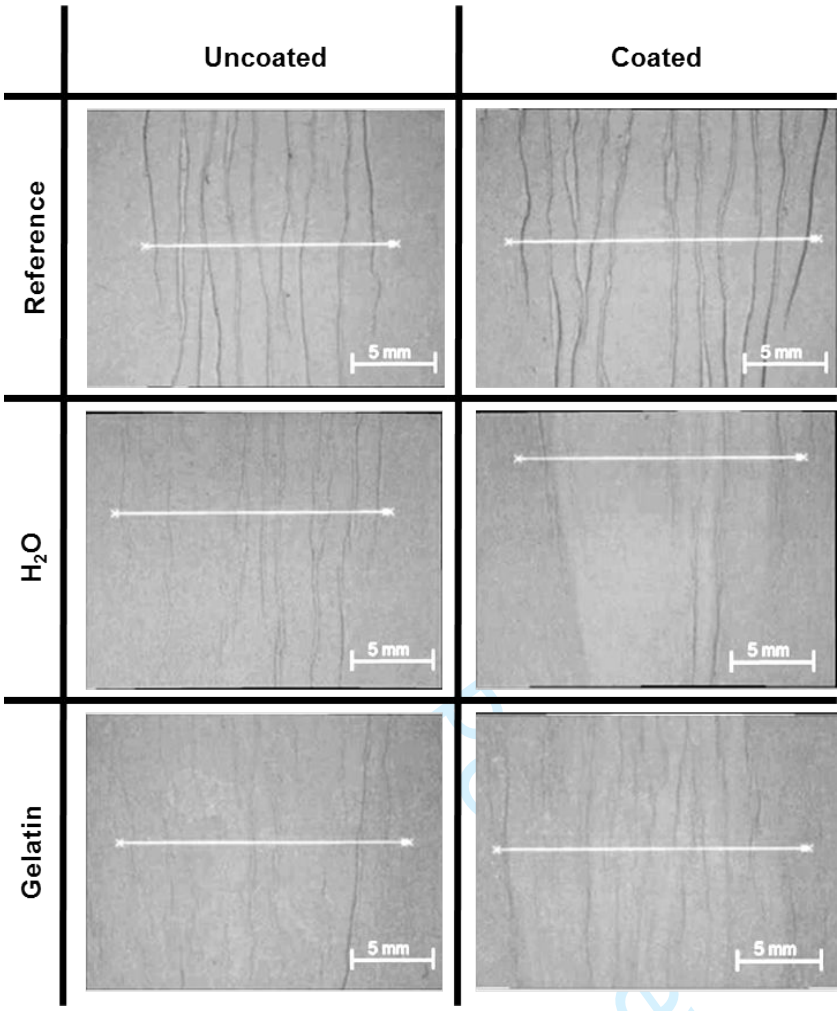

Figure 19: Wrinkling behaviour in the flange area of drawn cups

The optical findings in Figure 19 are corroborated by the roughness measurement presented in Figure 20. It shows the roughness R_a and R_z along the highlighted lines in Figure 19. The roughness proves that the R_a values decrease by adding water or treated water for the uncoated material, which is in line with the optical impression. The R_a value of the coated material does not seem to be affected positively by adding water. The value rather increases with adding water and stays at its origin with gelatin-treated water. Considering the R_z value, the roughness can be decreased by almost 80 % (uncoated) and around 35 % (coated) by adding gelatin or soap to the water. Treatment with pure water leads to a smaller decrease. The surface roughness is mostly related to the development of wrinkles in the flange area. Less roughness is connected to less wrinkles and a lower height of the wrinkles. Fewer wrinkles and the lower height of the wrinkles for the uncoated material can easily be associated with the higher moisture content of water-, gelatin- or soap-treated specimens. The moisture lowers the bending stiffness of the blanks and thus leads to more wrinkles with lower height. Additionally, the moisture content enables a better formability which leads to better compression of the wrinkles.

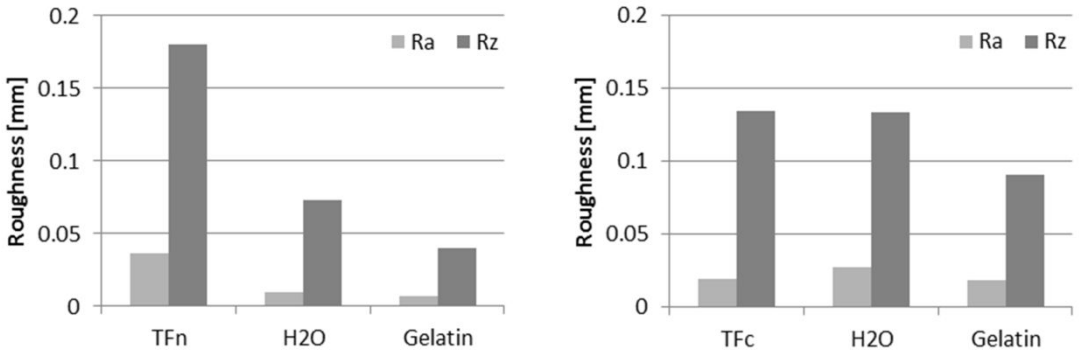

Figure 20: The roughness of the flange area of reference and treated blanks

In the bottom area of the treated shapes, it turns out that TFc tends to crinkle a delaminated coating. This occurs for every chosen treatment and is exemplarily shown in Figure 21 (on the right). Furthermore, it is measurable by the surface roughness, ranging from $R_a = 0.003$ mm and $R_z = 0.020$ mm (for the reference) to $R_a = 0.015$ mm and $R_z = 0.100$ mm (for water). This effect occurs due to the compression stress on the inside of the bottom of the drawing cups.

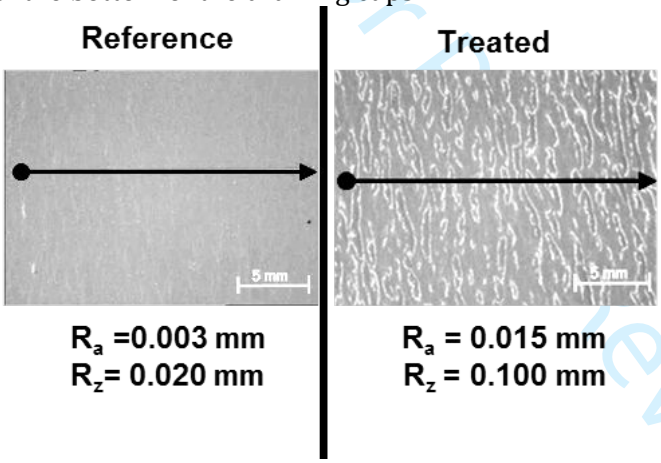

Figure 21: The inner surface of a drawn cup; on the left – the coated reference material; on the right – the treated material (an example for water, soap and gelatin treatment)

4. Conclusions and Outlook

The following conclusions can be drawn:

1. In tensile loading, the coated materials' strength is up to 15.5 % higher in the CD and up to 9.6 % higher in the MD compared with the combination of a separated coating and uncoated material in each direction. This is the result of the infiltration and mutual support of the fibre network and the coating.
2. The aforementioned effect depends on the loading state and is influenced by the different lateral elongation of the coating and the paperboard and does not occur in multi-axial stress states. A reason for that is the strain distribution of the coated material, which is more homogeneous due to the isotropic behaviour of the coating layer.
3. The treatment of the uncoated material by water, a soap solution and a gelatin solution affects the bearable strain (increasing) and forces (decreasing) in tensile and in biaxial loading differently.
4. The treatment has less influence on the coated material.

5. The drawing depth in the forming test can be assumed by the strength and bearable strain on the material in the bulge test. Gelatin solution–treated water supports the homogenisation of strain distribution in both directions (bulge test) by increasing the bearable strain in the MD. Thus it leads to the deepest drawing depth in the forming test.
6. The forming result can not only be described by the strength and bearable strain, it is necessary to take wrinkle distribution and surface quality into account.

Further investigations will consider the effect of temperature on the additive treated blanks and show how counter pressure will help to suppress wrinkling or to improve the surface quality. A more detailed analysis with, for example, a cyclic tensile test would further contribute to the understanding of the influence on elastic-plastic behaviour of the chosen treatment. Additionally, the friction behaviour will be considered to provide a deeper understanding of the mechanics of the tool and to better differentiate material behaviour from interaction.

5. Acknowledgements

The authors would like to thank the Research Foundation of LUT for participating in the funding of the work.

6. References

1. Leminen V, Tanninen P, Mäkelä P, Varis J. Combined effect of paperboard thickness and mould clearance in the press forming process. *Bioresources*. 2013;8(4):5701-5714.
2. Tanninen P, Kasurinen M, Eskelinen H, Varis J, Lindell H, Leminen V, Matthews S, Kainusalmi M. The effect of tool heating arrangement on fibre material forming. *Journal of Materials Processing Technology*. 2014;214(8):1576-1582.
3. Hauptmann M, Weyhe J, Majschak J-P. Optimisation of deep drawn paperboard structures by adaptation of the blank holder force trajectory. *Journal of Materials Processing Technology*. 2016;232:142-152.
4. Leminen V, Tanninen P, Lindell H, Varis J. Effect of blank holding force on the gas tightness of paperboard trays manufactured by the press forming process. *Bioresources*. 2015;10(2):2235-2243.

5. Groche P, Huttel D. Paperboard forming – Specifics compared to sheet metal forming. *Bioresources.* 2016;11(1):1855-1867.
6. Stein P, Franke W, von Elling M, Groche P. Forming behaviour of paperboard in single point incremental forming. *Bioresources*. 2019;14(1):1731-1764.
7. Vishtal A, Khakalo A, Retulainen E. Extensible cellulosic fibre-polyurethane composites prepared via the papermaking pathway. *Bioresources.* 2018;13(3):5360-5376.
8. Vishtal A, Retulainen E. Boosting the extensibility potential of fibre networks: A review. *Bioresources.* 2014;9(4):7951-8001.
9. Hauptmann M, Wallmeier M, Erhard K, Zelm R, Majschak J-P. The role of material composition, fiber properties and deformation mechanisms in the deep drawing of paperboard. *Cellulose.* 2015;22:3377-3395.
10. Jambeck JR et al. Plastic waste inputs from land into the ocean. *Science*. 2015;347 (6223):768-771.
11. Hauptmann M, Weyhe J, Majschak J-P. Optimisation of deep drawn paperboard structures by adaptation of the blank holder force trajectory. *Journal of Materials Processing Technology*. 2016;232:142-152.
12. Tanninen P, Leminen V, Matthews S, Kainusalmi M, Varis J. Process cycle optimization in press forming of paperboard. *Packag Technol Sci.* 2017;:1-8.
13. Hauptmann M, Majschak JP, New quality level of packaging components from paperboard through technology improvement in 3D forming. *Packaging Technology and Science*. 2011;24(7):419-432.
14. Östlund M, Borodulina S, Östlund S. Influence of paperboard structure and processing conditions on forming of complex paperboard structures. Pack Technol Sci. 2011;24(6):331-341.

15. Scherer K. *Das Ziehen von Pappe: Untersuchungen über die Ziehfähigkeit und den Ziehvorgang von Pappe*, Papier-Zeitung Verlagsgesellschaft mbH, Berlin, Germany; 1935.
16. Franke W, Stein P, Dörsam S, Groche P. Formability of paperboard during deep-drawing with local steam application. In: ESAFORM 2018, 23.04.-25.04.2018, Palermo, Italy.
17. Khakalo A et al. Using gelatin protein to facilitate paper thermoformability. *Reactive and Functional Polymers.* 2014;85:175-184.
18. Khakalo A, Filpponen I, Rojas OJ. Protein adsorption tailors the surface energies and compatibility between polylactide and cellulose nanofibrils. *Biomacromolecules.* 2017;18(4):1426-1433.
19. Vishtal A, Khakalo A, Rojas OJ, Retulainen E. Improving the extensibility of paper: Sequential spray addition of gelatine and agar. *Nordic Pulp & Paper Research Journal.* 2015;30(3);452-460.
20. Huttel D, Post P, Schabel S, Groche P. The stress strain behavior of paperboard in tensile and bulge tests. Paper presented at: Proceedings of the 10th International Conference on Technology of Plasticity; 2011.
21. Tanninen P, Ovaska S-S, Matthews S, Mielonen K, Backfolk K. Utilization of production-scale machine in experimental fiber material convertibility testing using a novel press-forming tool set. *Bioresources.* 2017;12(2):3030-3042.
22. Hauptmann M, Schult A, Zelm R, Gailat T, Lenske A, Majschak J-P, Großmann H. Gastight paperboard package – A new step in food packaging. *Professional Papermaking.* 2013;1:48-51.
23. Leminen V, Tanninen P, Ovaska S-S, Varis J. Convertability and oil resistance of paperboard with hydroxylpropyl-cellulose-based dispersion barrier coatings. *Journal of Applied Packaging Research*. 2015;7:91-100.

24. Tanninen P, Saukkonen E, Leminen V, Lindell H, Backfolk K. Adjusting the die cutting process and tools for biopolymer dispersion coated paperboards. *Nordic Pulp & Paper Research Journal*. 2015;30(2):336-343.

25. Tanninen P, Lindell H, Saukkonen E, Backfolk K. Thermal and mechanical durability of starch-based dual polymer coatings in the press forming of paperboard. *Packaging Technology and Science.* 2014;27:353-363.

26. De Ruvo A, Carlsson L, Fellers C. The biaxial strength of paper. *TAPPI Journal.* 1980;63:133-136.

27. Wahlström T, Fellers C. Biaxial straining of paper during drying, relations between stresses, strains and properties. Paper presented at: TAPPI Engineering Conference 1999; 705-720.

28. Linvill E, Östlund S. Biaxial in-plane yield and failure of paperboard. *Nordic Pulp and Paper Research Journal*. 2016;31:659-667.

29. **Table 1: The ratio of Young's modulus, tensile strength and strain at breakage in different directions**

	Value	Reference	H_2O	Soap	Gelatin
TFc	$\frac{E_{CD}}{E_{MD}}$	0.43	0.16	0.19	0.25
	$\frac{\sigma_{max,CD}}{\sigma_{max,MD}}$	0.43	0.51	0.54	0.51
	$\frac{\epsilon_{max,CD}}{\epsilon_{max,MD}}$	2.42	3.03	2.71	2.80
TFn	$\frac{E_{CD}}{E_{MD}}$	0.37	0.25	0.26	0.29
	$\frac{\sigma_{max,CD}}{\sigma_{max,MD}}$	0.41	0.45	0.48	0.42
	$\frac{\epsilon_{max,CD}}{\epsilon_{max,MD}}$	2.84	2.79	3.21	3.17

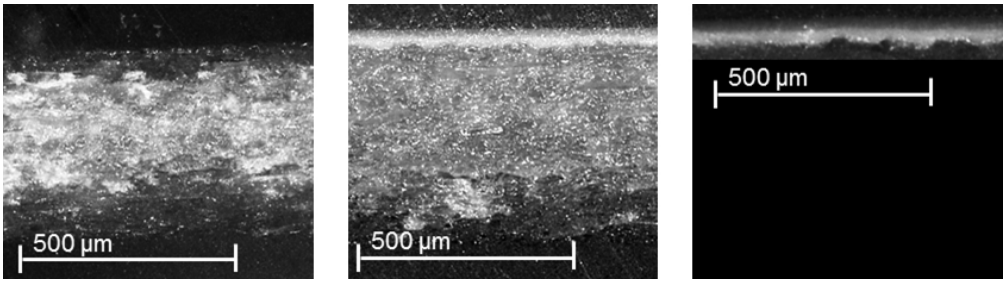

Figure 1: Images of the material section: TFn (left), TFc (middle) and the PET coating (right)

71x19mm (300 x 300 DPI)

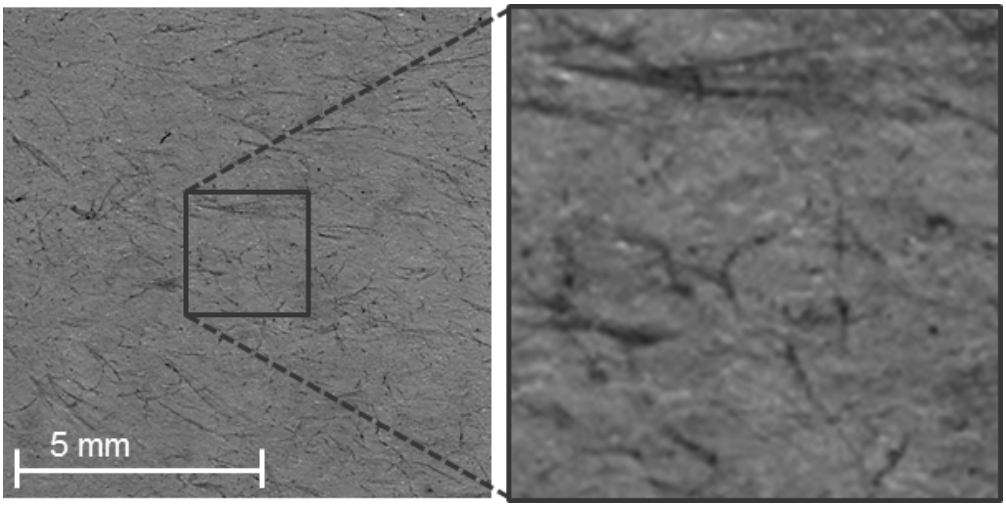

Figure 2: The surface of the separated coating layer (view from the former paperboard side)

51x25mm (300 x 300 DPI)

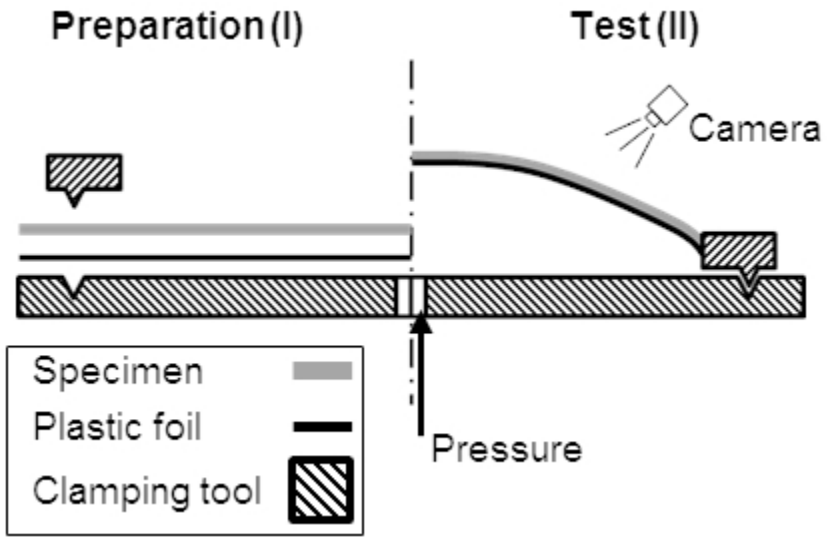

Figure 3: The schematic bulge test setup

9x5mm (1200 x 1200 DPI)

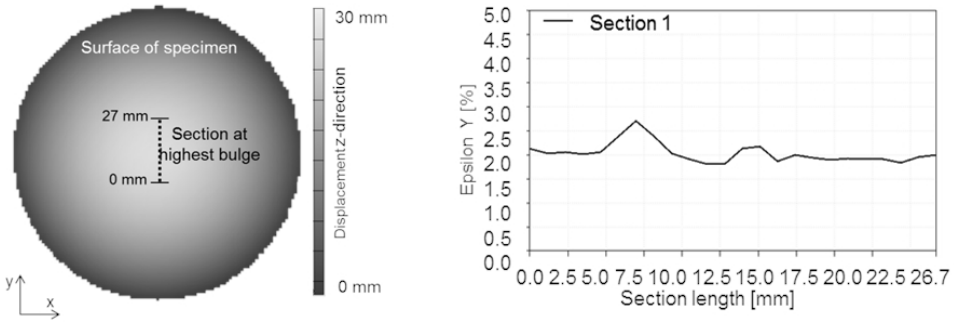

Figure 4: The definition of the section and calculation of the mean value of strain – section adjustment by displacement in a z direction (left) and calculation of the mean value (strain) along the section (right)

78x25mm (300 x 300 DPI)

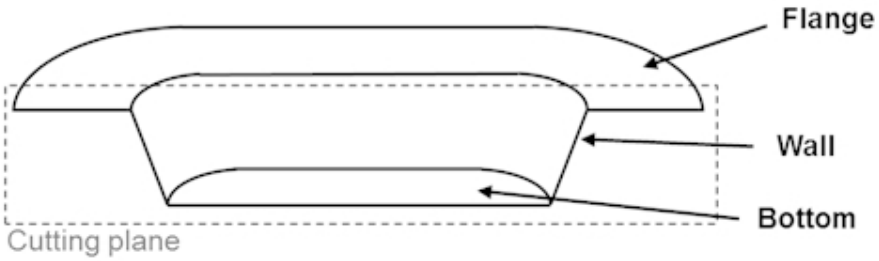

Figure 5: A schematic definition of the drawing test parts

45x13mm (300 x 300 DPI)

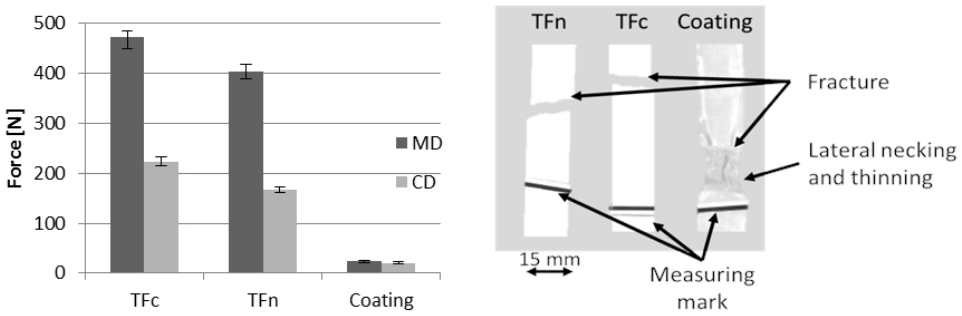

Figure 6: Average force at break of the tensile tests of TFc, TFn and the coating in an MD and CD (left) and the exemplary fracture areas of TFn, TFc and the coating (right)

75x25mm (300 x 300 DPI)

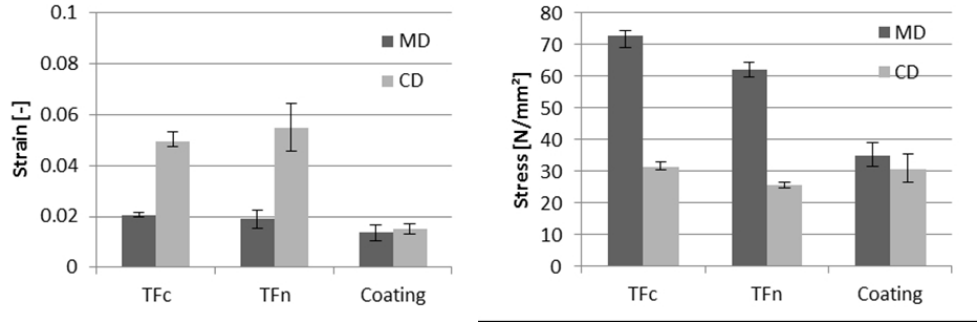

Figure 7: Average strain and stress at break of the tensile test of TFc, TFn and coating in the MD and CD for room conditions

20x6mm (1200 x 1200 DPI)

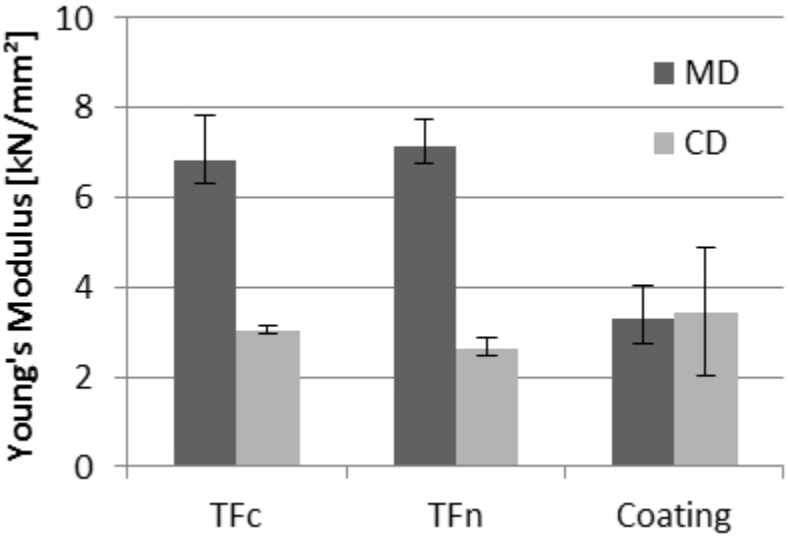

Figure 8: Young's modulus of the reference materials

9x6mm (1200 x 1200 DPI)

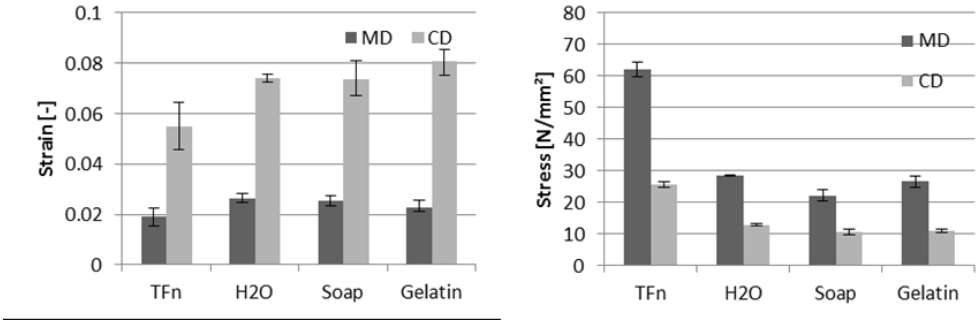

Figure 9: Average strain and stress at break of tensile tests of the uncoated reference material (TFn) and the treated materials (H2O; soap; gelatin)

18x6mm (1200 x 1200 DPI)

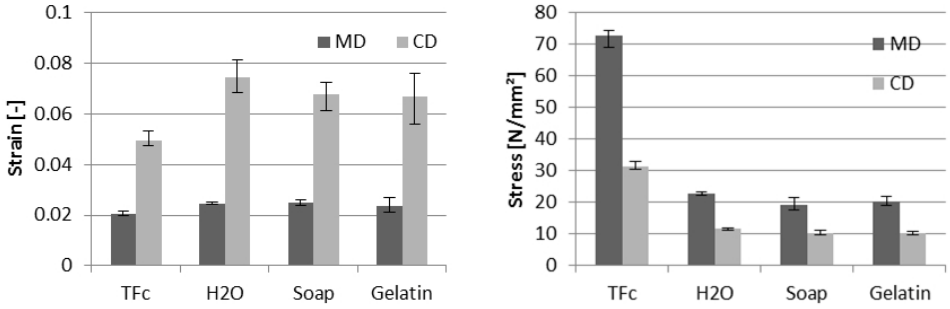

Figure 10: Average strain and stress at break of the tensile tests of coated reference (TFc) and treated materials (H2O; Soap; Gelatin)

18x6mm (1200 x 1200 DPI)

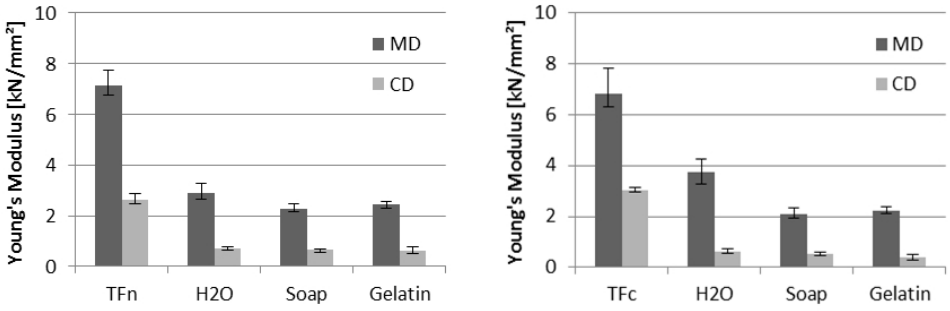

Figure 11: The Young's moduli of the references (TFn; TFc) and the treated materials (H2O; soap; gelatin)

18x6mm (1200 x 1200 DPI)

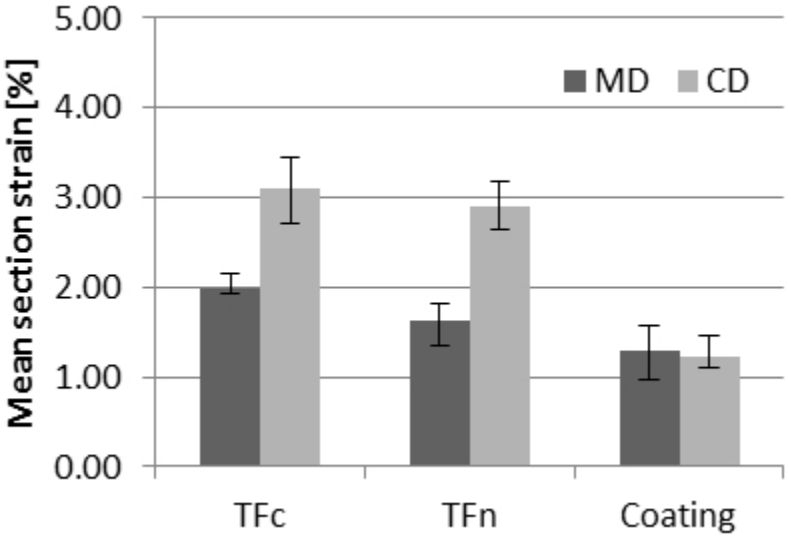

Figure 12: The values of the average strain along the section through the bulge before it bursts in a bulge test

9x6mm (1200 x 1200 DPI)

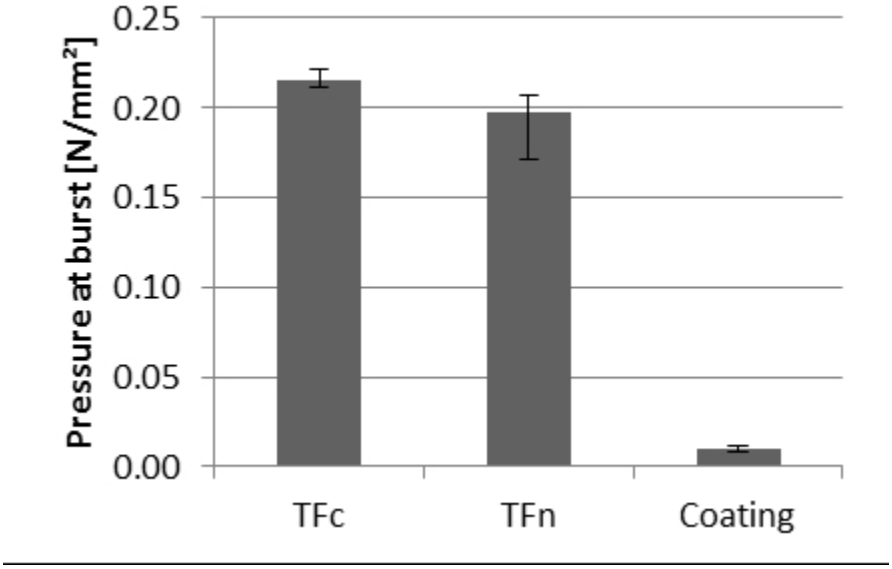

Figure 13: Pressure before burst in the bulge test for each layer and superimposing

9x6mm (1200 x 1200 DPI)

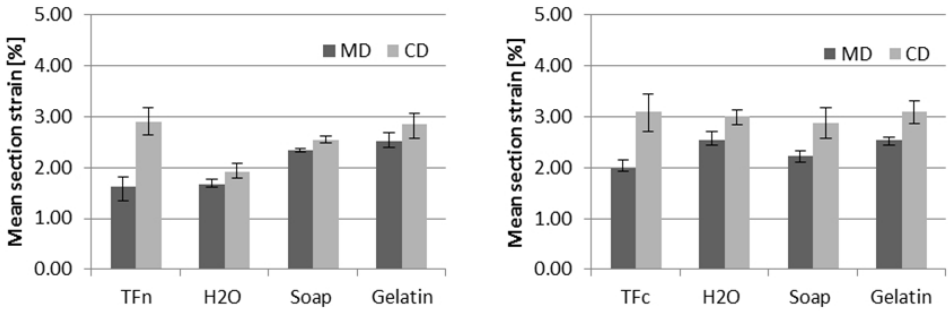

Figure 14: The bulge test results for the treated materials' strain

18x6mm (1200 x 1200 DPI)

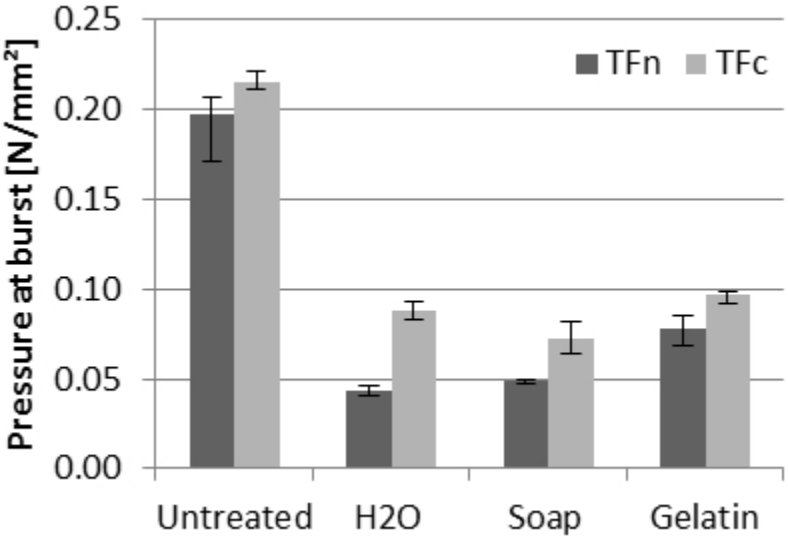

Figure 15: The bulge test results for treated materials strain

9x6mm (1200 x 1200 DPI)

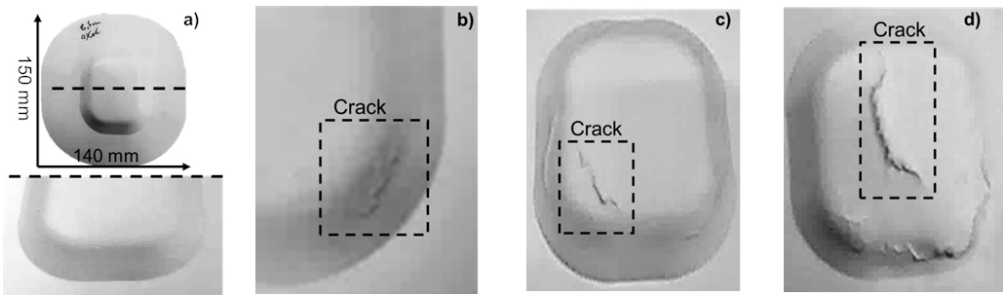

Figure 16: The fracture behaviour of the formed parts compared with parts without cracks (a), with a crack in the top layer at the flange (b), with a crack through several layers on the top (c) and with a crack through the whole thickness (d)

361x106mm (72 x 72 DPI)

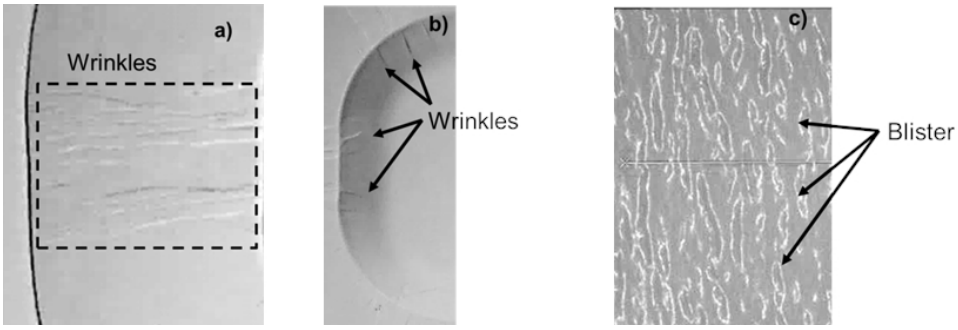

Figure 17: Product imperfections after forming: wrinkles in the flange area (a) and cup wall (b), and a blistering pattern in the bottom area (c)

72x23mm (300 x 300 DPI)

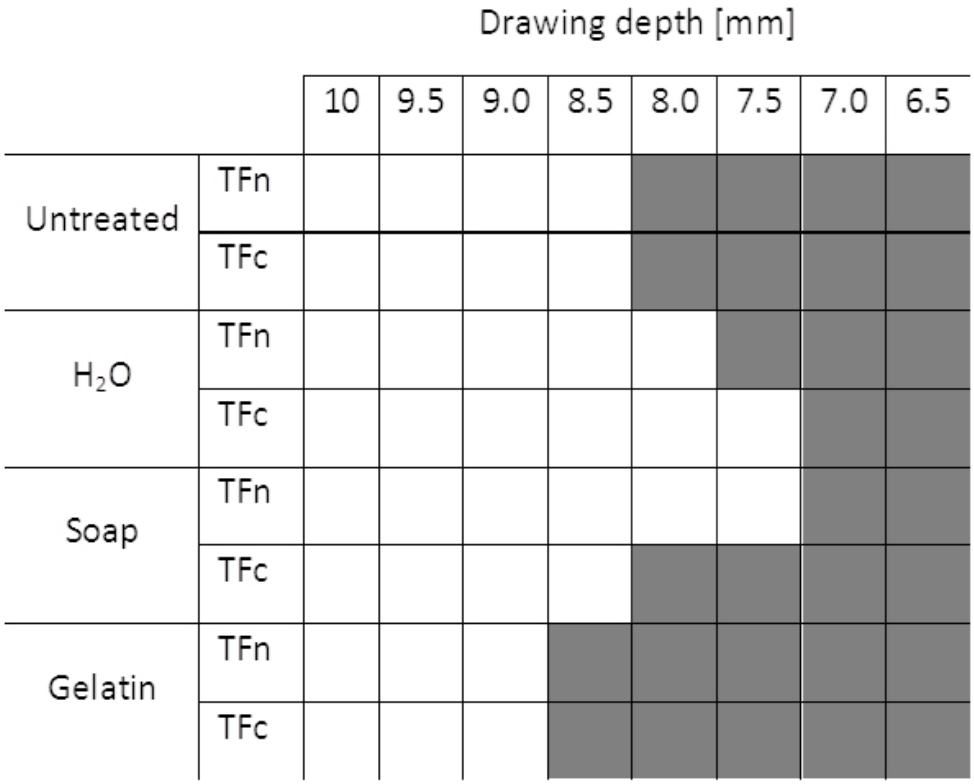

Figure 18: The forming test results for 10 mm to 6.5 mm drawing depth and all the treated and reference materials; white = failure/crack; grey = no failure/crack

12x11mm (1200 x 1200 DPI)

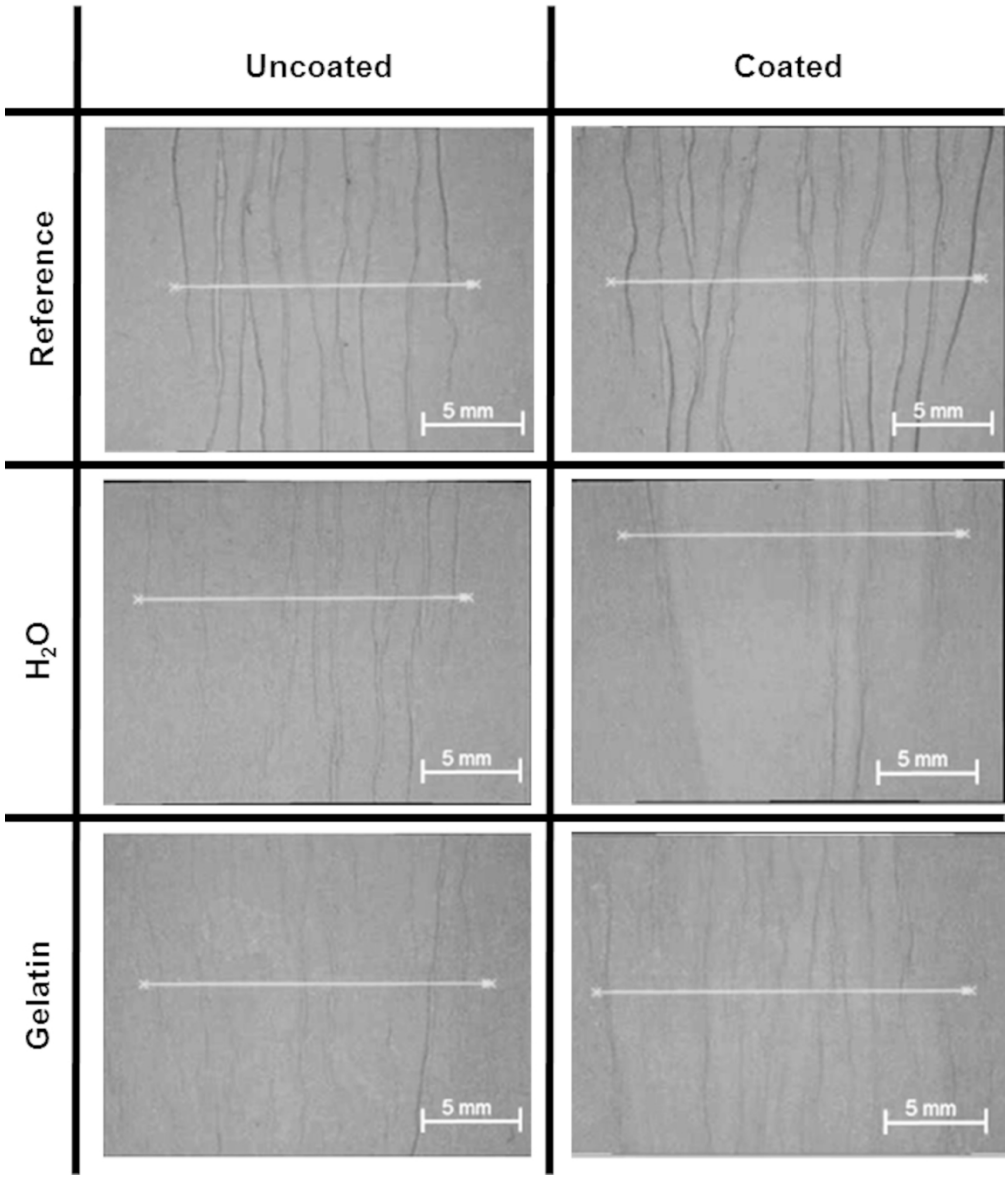

Figure 19: Wrinkling behaviour in the flange area of drawn cups

122x143mm (300 x 300 DPI)

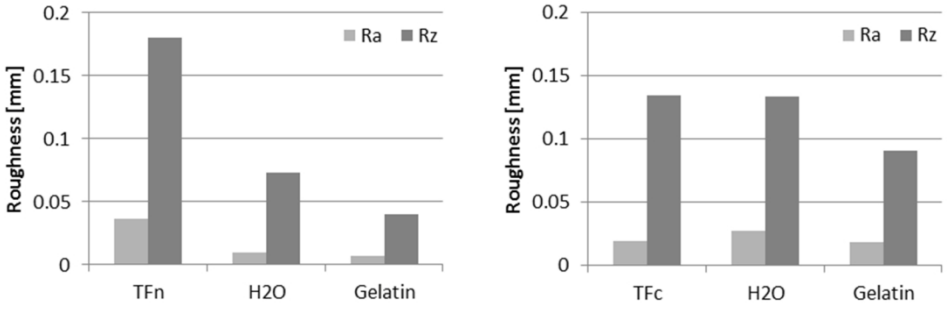

Figure 20: The roughness of the flange area of reference and treated blanks

37x12mm (1200 x 1200 DPI)

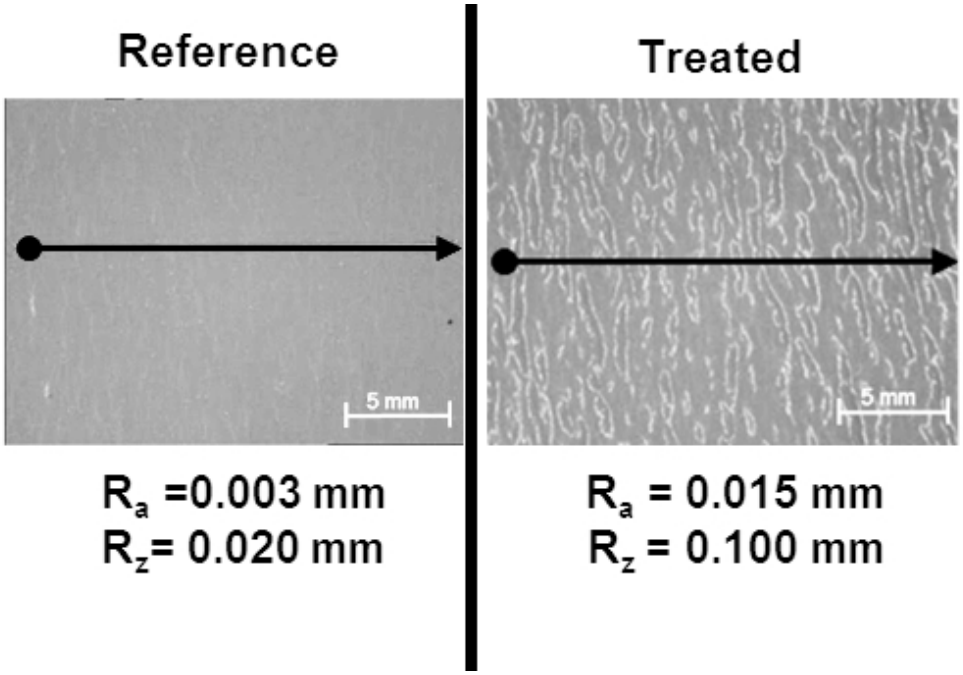

Figure 21: The inner surface of a drawn cup; on the left – the coated reference material; on the right – the treated material (an example for water, soap and gelatin treatment)

43x28mm (300 x 300 DPI)